Failure Load of Frp Strengthened Masonry Walls: Experimental Results and Numerical Models

G. Milani[1], T. Rotunno[2], E. Sacco[3] and A. Tralli[1,4]

Abstract: Aim of the present work is the evaluation of the ultimate load bearing capacity of masonry panels reinforced with FRP strips. The investigation is developed performing both experimental and numerical studies. In particular, several panels subjected to different loading conditions are tested in the Tests Laboratory of the University of Florence (Italy). Then, numerical models based on combined homogenization and limit analysis techniques are proposed. The results obtained by numerical simulations are compared with experimental data. The good agreement obtained shows that the proposed numerical model can be applied for the evaluation of the ultimate load bearing capacity of reinforced masonry walls.

keyword: Masonry, FRP strengthening, Homogenization, Limit analysis, FE models.

1 Introduction

The development and the use of new technologies and materials for both restoring and reinforcing masonry structures are technically and economically very interesting (Di Tommaso 2000). In particular, fiber reinforced polymers (FRP) have been already widely applied in several cases of technical relevance. As a matter of fact, in Italy the recent seismic events in Umbria and Marche in 1997-1998 led to accelerate the use of these materials on existing masonry structures, because of the remarkable lightness, non invasiveness and reversibility which characterize this technology of consolidation (Corradi, Borri and Vignoli 2002). FRP materials – which are typically made of Carbon (CFRP) and Glass (GFRP) fibers bonded together with polymeric two-components epoxy resin – offer to the designer a combination of properties, including high strength in the direction of fibers, immunity of corrosion, low weight and availability in form of laminates, fabrics and tendons of practically unlimited length.

The research in this field was originally carried out in U.S. and Japan where the first applications on concrete structures were performed in the 1990's. Afterwards, interest focused also on masonry constructions and Schwegler (1994) and Triantafillou and Fardis (1997) developed experimental researches on the behavior of brickwork reinforced with CFRP.

A recent overview of research studies and application fields on masonry strengthening with FRP composites has been presented by Nanni and Tumialan (2003); they discussed experimental results regarding both the in- and out-of-plane behavior of walls, with issues related to design for the benefit of practicing engineers.

In order to predict the increasing of the load bearing capacity of masonry walls obtained by the introduction of FRP strips, non-linear analysis methods should be used. In fact, effective stress analyses of reinforced masonry structures should consider the brittle behavior in traction of masonry, the limited strength of masonry in compression accompanied by inelastic strains and damage effects, the activation of possible delamination phenomena of the FRP from the brickwork and the brittle failure of the reinforcement.

A further difficulty specific of the masonry modeling is due to its heterogeneous character, since it is composed of blocks joined together by thin layers of mortar. Nevertheless, in many cases of technical relevance, blocks are regularly disposed and this allows, in the framework of homogenization, to substitute, at a structural level, bricks and mortar with a macroscopic homogeneous material, once that a suitable boundary value problem is solved at a cell level.

Non-linear homogenization procedures for the analysis

---

[1] ENDIF, ENgineering Department In Ferrara, Università di Ferrara, Via Saragat 1, 44100 Ferrara, Italy.

[2] Dipartimento di Costruzioni, Università di Firenze, Piazza Brunelleschi 6, Firenze, Italy.

[3] Dipartimento di Meccanica Strutture Ambiente e Territorio, Università di Cassino, Via Di Biasio 43, Cassino, Italy.

[4] A short version of this paper was presented at the XXXIV Conference of the Italian Association for Stress Analysis (AIAS), Milan Italy 14-17 September 2005.
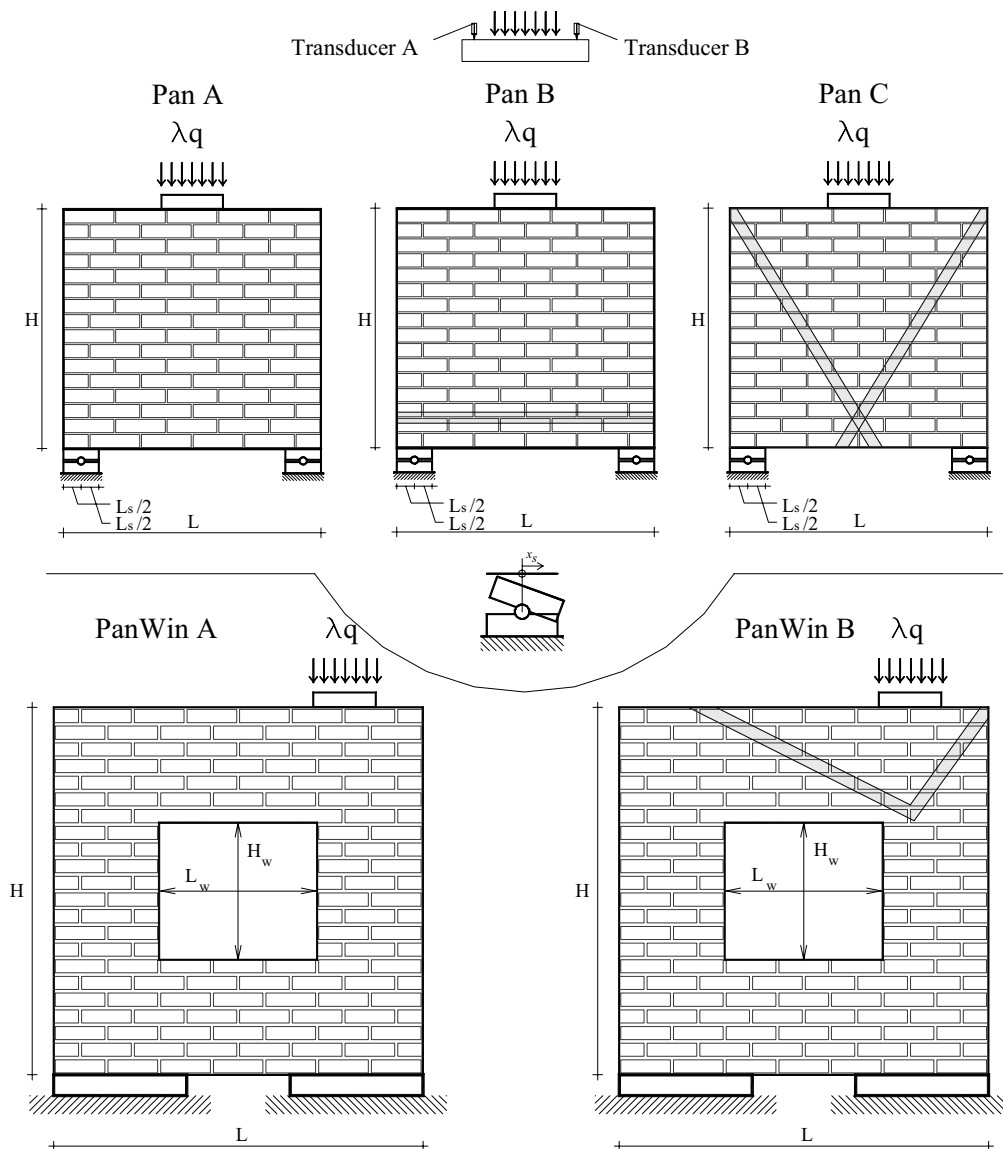
Figure 1 : Panels series experimentally tested.

of reinforced masonry have been proposed by Luciano and Sacco (1998) and by Marfia and Sacco (2001), where damages of the mortar layer, of the block and of the masonry-FRP interface are considered.

The typical strain softening behavior of the reinforced masonry structures precludes, in principle, the use of the classical limit analysis theorems. Nevertheless, incremental step by step procedures could provide results strongly dependent on the load process, on the presence of self stress states and on the mechanical material parameters, which could vary from point to point and could be difficult to evaluate. Furthermore, it has been shown

that simple at hand calculations based on limit analysis (Limam, Foret and Ehrlacher 2003) give reliable estimations of experimental collapse loads of FRP reinforced concrete slabs; as consequence, the limit analysis can represent a useful tool for designers and practitioners to evaluate the ultimate load bearing capacity of reinforced masonry structures.

Thus, the limit analysis combined with a homogenization technique appears to be a powerful structural analysis tool to predict masonry behavior at collapse in presence of FRP reinforcements. This approach requires only a reduced number of material parameters, it allows to avoid

Table 1 : Mortar compressive strength.

M1 MPa	M2 MPa	M3 MPa	M4 MPa	M5 MPa	M6 MPa	f_{M-m} MPa	s_M MPa
2.0	2.24	2.18	2.13	2.1	2.13	2.13	0.08
f_{M-m}	Average compressive strength						
s_M	Standard deviation						

Table 2 : Bricks compressive strength.

B1 MPa	B2 MPa	B3 MPa	B4 MPa	B5 MPa	B6 MPa	B7 MPa	B8 MPa	B9 MPa	B10 MPa
16.2	17.7	14.8	18.6	13.7	12.1	12.9	15.8	19.1	15.7
f_{b-m}	15.66	MPa	Average compressive strength						
s_b	2.49	MPa	Standard deviation						

independent modeling of units and mortar and it is able to provide limit multipliers of loads, failure mechanisms and, at least on critical sections, the stress distribution at collapse.

In the present work, an experimental investigation on the behavior of reinforced masonry elements is developed. Then, a numerical procedure based on the limit analysis within a homogenization technique is proposed. The results obtained by means of numerical models based on combined homogenization-limit analysis techniques are compared with experimental data for several panels reinforced in different ways.

In Section 2 the experimental set-up of the tests is described in detail, whereas in Section 3 the homogenization procedure adopted for obtaining macroscopic failure surfaces for unreinforced masonry is developed.

In Section 4 lower and upper bound FE limit analyses formulations applied to masonry panels reinforced with FRP strips are proposed.

Finally, in Section 5 comparisons between numerical and experimental results are discussed.

2 Experimental tests

2.1 Panels geometry and loading conditions

Experimental tests were performed for five different masonry walls series (series Pan A, Pan B, Pan C, PanWin A and PanWin B).

In particular, 9 panels of dimensions 290x270 mm^2 ($L \times H$) and 3 panels of dimensions 416x414 mm^2 ($L \times H$) with a central hole of dimensions 184x156 mm^2 ($L_w \times H_w$), as illustrated in Figure 1, were tested for Pan series and PanWin series, respectively. All the panels were built by means of little clay bricks of dimensions 56x15 mm^2 (length×height) and cement-lime mortar joints, being the thickness t of the walls equal to 30 mm.

3 samples were tested for Pan A, Pan B and Pan C series, respectively, whereas only 1 sample PanWin A and 2 samples Pan Win B were loaded until failure.

Series Pan A, Pan B and Pan C were placed on two steel plates of length $L_s = 40$ mm disposed at the lower edge corners and positioned on little steel rollers allowing rotation of the supports (Figure 1). Series PanWin A and PanWin B were placed on two steel plates positioned directly upon a stiff steel beam, in order to preclude rotation of the supports.

CFRP strips of width $l_w = 12.5$ mm and symmetrically disposed on the two surfaces of the masonry panels were introduced in series Pan B, Pan C and PanWin B, as shown in Figure 1. Loading conditions for all the series of panels are shown in Figure 1. Loads were applied upon a partitioning steel plate of dimensions 70x30 mm^2 and making use of a suitable displacement control device.

Loads were registered by means of a 100 kN load cell, whereas prescribed displacements were registered with two symmetrically disposed transducers A and B placed in correspondence of the loads, as shown in Figure 1.

Table 3 : Masonry compressive strength.

Ma1 MPa	Ma2 MPa	Ma3 MPa	Ma4 MPa	Ma5 MPa	Ma6 MPa	f_{m-m} MPa	s_m MPa
7.16	5.7	6.63	7.72	6.58	6.8	6.76	0.67
f_{m-m}	Average compressive strength						
s_m	Standard deviation						

Table 4 : Mechanical characteristics adopted in the numerical simulations.

	γ N/m^3	E MPa	f_c MPa	f_t MPa
Mortar	18000	133	2.13	0.2
Brick	20000	1785	15.6	1.5
Masonry	-	830	6.76	-

2.2 Materials mechanical characteristics

Uniaxial compression tests were conducted on bricks, mortar and masonry specimens in order to determine materials compressive strengths. Tests were conducted in agreement with the Italian code of practice D.M. 20/11/1987.

For lime-cement mortar, classified by the Italian code as M4, preliminary bending tests were conducted on 3 specimens of dimensions 40x40x160 mm^3, according to the Italian code D.M. 3/6/1968 requirements. The resulting 6 samples obtained after failure in bending were finally tested to uniaxial compression. Experimental results, average compressive strength and standard deviation (series M) are shown in Table 1.

Bricks were tested directly to compression making use of 10 samples of dimensions 56x15x30 mm^3 (length×height×width). Experimentation results, average compressive strength and standard deviation are shown in Table 2 (series B).

Finally, compression tests for masonry required the construction of 6 samples (series Ma) of dimensions 114x104x30 mm^3, in agreement with D.M. 20/11/1987. The values of compressive strength obtained experimentally for all the samples, average value of compressive strength and standard deviation are reported in Table 3.

Characteristic values f_k of compressive strength for masonry can be obtained in agreement with D.M.

20/11/1987 as follows:

$$f_k = f_m - ks = 5.2 \text{ (MPa)} \tag{1}$$

with $k = 2.33$.

It is worth noting that tensile strength is estimated, as commonly accepted, to be 1/10 of compressive strength.

A synopsis of the mechanical parameters values adopted in the following for the numerical simulations is presented in Table 4, where γ is the bulk density, E is the Young's modulus, f_c is the compressive strength and f_t is the tensile strength.

Table 5 : Mbrace System (MAC S.p.A.).

	γ N/m^3	E MPa	f_t MPa
Fiber C1-30	18200	230000	3430
Matrix	10200	3000	50

CFRP strips used for Pan B, Pan C and PanWin B series were constituted by "Mbrace Fibers C1-30" high-strength carbon fiber ribbons and a two-component epoxy-base matrix, whose technical specifications were furnished by MAC S.p.A (Table 5)

The testing equipment was designed and manufactured at the Tests Laboratory of the University of Florence.

A critical discussion of tests results, i.e. experimental failure mechanisms, crack patterns and delamination phenomena observed are reported in Section 5.
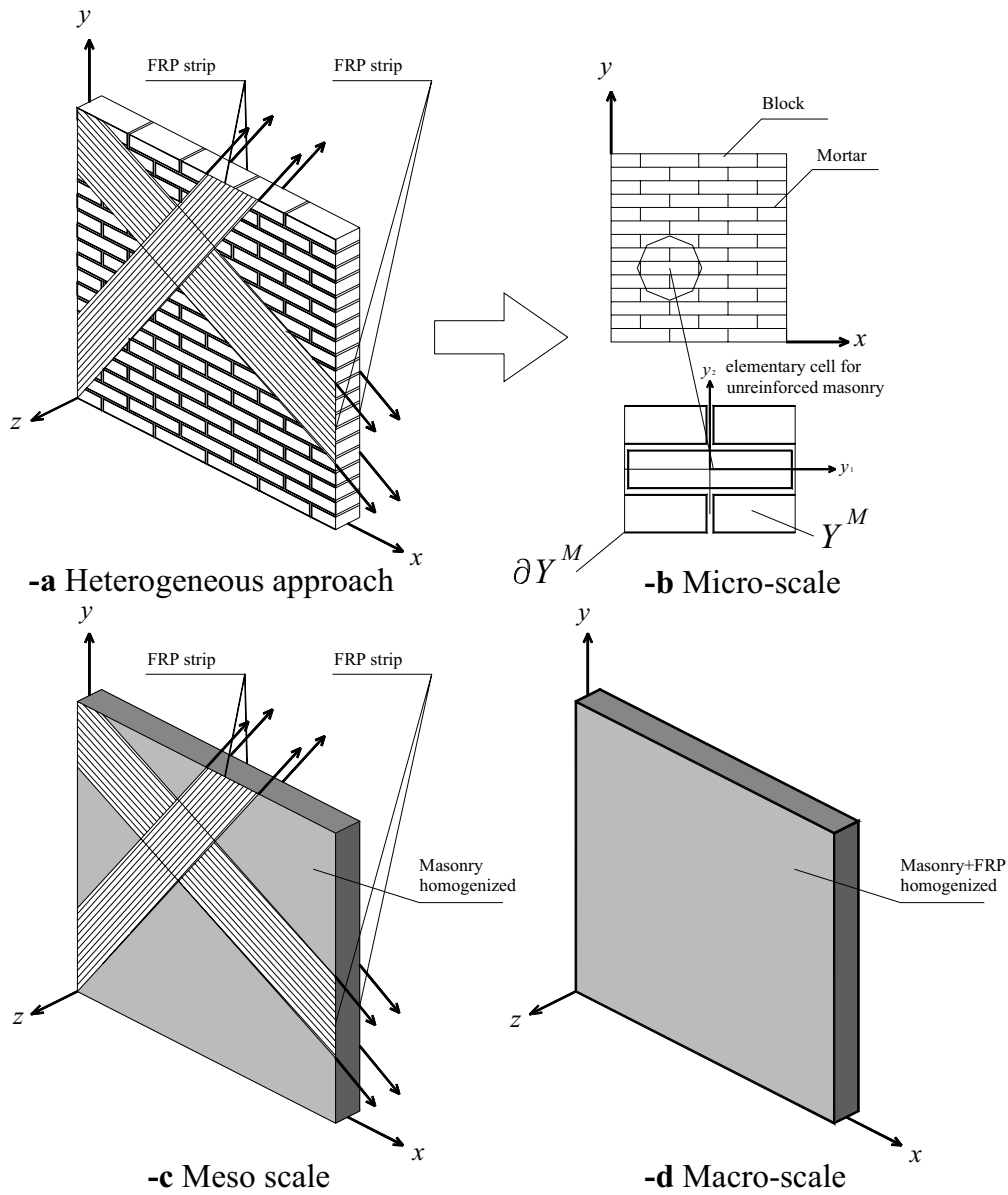
Figure 2 : Possible models for the analysis at collapse of reinforced masonry walls. –a: heterogeneous model; -b: micro-scale approach; -c: meso-scale approach; -d: macro-scale full homogenized approach.

3 Analysis at collapse of masonry walls reinforced with FRP: brickwork failure surfaces

In this Section, a homogenization approach for deriving brickwork failure surface is presented. A lower bound approach is adopted, which consists in assuming polynomial distributions for the micro-stress field in a suitable number of sub-domains in the unit cell and in imposing both equilibrium and admissibility conditions for the constituent materials. In this way, a lower bound estimation of the masonry failure surface is obtained (*cell*

level). Such strength domain is then implemented both in lower and upper bound FE limit analyses codes (see Section 4), in order to perform static and kinematic analyses at collapse of entire panels reinforced with FRP strips (*structural level*).

The introduction of FRP external layers on masonry (Figure 2-a) is treated by means of a simplified *multi step* approach. In the first step, –*micro-scale* (Figure 2-b)- unreinforced masonry is studied by means of suitable homogenization techniques, for a periodic unit cell. In this way,
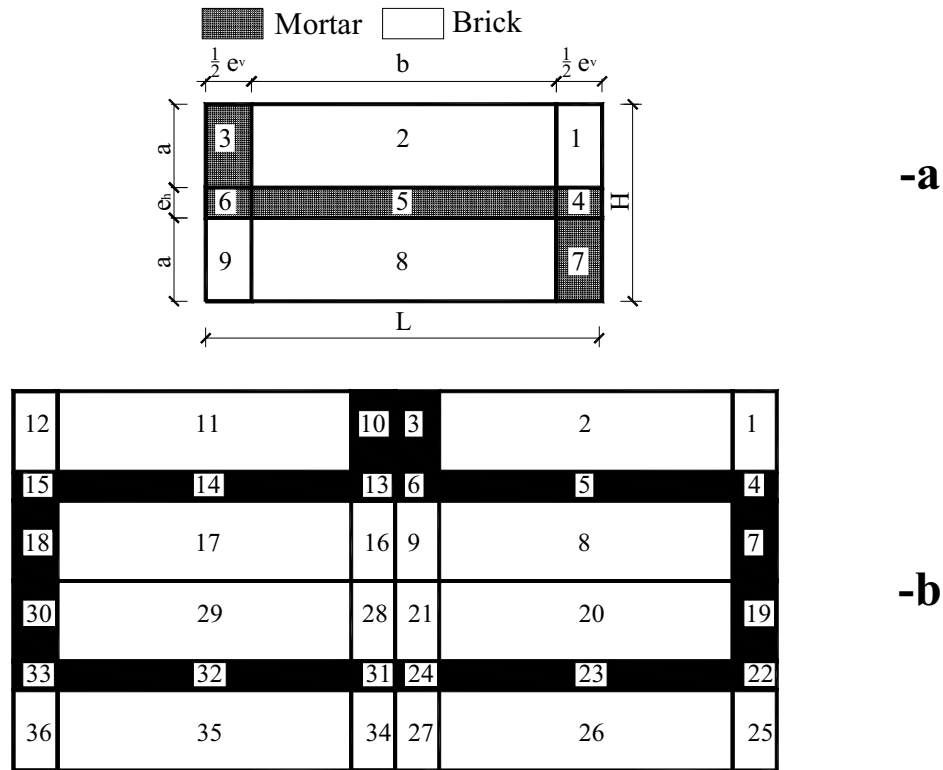
Figure 3 : Subdivision in sub domains adopted. –a: subdivision and geometrical characteristics of one-fourth of the elementary cell. –b: subdivision into 36 sub-domains for the entire cell.

an estimation of the homogenized unreinforced masonry strength domain is obtained and masonry is substituted with an equivalent macroscopic homogeneous material. In the second step –*meso-scale* (Figure 2-c)- FRP reinforcement strips are introduced, in the framework of a multi-layer approach, on the already homogenized masonry material.

A *macro-scale* analysis could also be developed (Cecchi, Milani and Tralli 2004 and Figure 2-d), considering the FRP reinforcement diffused on the entire external brickwork surfaces. Nevertheless, this procedure cannot be considered in practice when the reinforcement typology consists in the application of strips and/or pultruded laminates.

When a *meso-scale* approach is adopted, the homogenized strength domain for unreinforced masonry can be recovered solving a suitable yield boundary problem on the periodic unit cell. At this aim, both static and kinematic approaches (de Buhan and de Felice 1997) could be developed. Following Milani, Lourenço and Tralli (2006a), in this study only the static approach is

adopted, providing a lower bound estimation of the masonry strength domain.

Adopting an associated flow rule for the constituent materials, Suquet (1983) proved that a lower bound approximation of the mesoscopic strength domain $S_{meso-scale}^{hom}$ of the unreinforced masonry can be obtained solving the following problem:

$$S_{meso-scale}^{hom}$$

$$= \begin{cases} \Sigma = \langle \sigma(\mathbf{y}) \rangle = \frac{1}{|Y^M|} \int\limits_{Y^M} \sigma(\mathbf{y}) \, dY^M \quad (a) \\ \\ \sigma(\mathbf{y}) \cdot \mathbf{n}(\mathbf{y}) \quad \text{antiperiodic on } \partial Y^M \quad (b) \\ \\ div\sigma(\mathbf{y}) = \mathbf{0} \quad \text{on } Y^M \quad (c) \\ \\ \text{with} \begin{cases} \sigma(\mathbf{y}) \in S^{block} \; \forall \mathbf{y} \in block \\ \\ \sigma(\mathbf{y}) \in S^{mortar} \quad \forall \mathbf{y} \in mortar \quad (d) \end{cases} \end{cases} \quad (2)$$

Where Y^M and ∂Y^M are the periodic cell (bricks + mortar joints) and its boundary (Figure 2-b); $\langle \cdot \rangle$ is the av-

erage operator, S^{block} and S^{mortar} represent the bricks and the mortar strength domains, respectively. Condition (2) (a) defines the mesoscopic stress $\mathbf{\Sigma}$ as an average of the microscopic stress $\mathbf{\sigma}$ on the periodic cell, whereas condition (2) (b) represents the continuity of the micro-stress vector between two adjacent unit cells. Condition (c) imposes micro-equilibrium on the cell and condition (d) represents the strength requirement – material admissibility - respectively for blocks and mortar.

In order to have a simple and efficient estimation of masonry homogenized failure surfaces, the simplified micro-mechanical model proposed by Milani, Lourenço and Tralli (2006a) is adopted to solve problem (2) in an approximated way. As shown in Figure 3, one-fourth of the periodic unit cell is sub-divided into nine geometrical elementary entities (*sub-domains*), so that all the cell is sub-divided into 36 sub-domains. The subdivision adopted is the coarser (for $1/4$ of the cell) that can be obtained using rectangular geometries for each sub-domain.

Polynomial distributions of degree m are *a priori* assumed for the stress components within each sub-domain. Since stresses are polynomial expressions, the generic ij^{th} component can be written as:

$$\sigma_{ij}^{(k)} = \mathbf{X}(\mathbf{y})\mathbf{S}_{ij}^{T} \quad \mathbf{y} \in Y^k \tag{3}$$

where: - $\mathbf{X}(\mathbf{y}) = \begin{bmatrix} 1 & y_1 & y_2 & y_1^2 & y_1 y_2 & y_2^2 & \dots \end{bmatrix}$;

- $\mathbf{S}_{ij} = \begin{bmatrix} S_{ij}^{(1)} & S_{ij}^{(2)} & S_{ij}^{(3)} & S_{ij}^{(4)} & S_{ij}^{(5)} & S_{ij}^{(6)} & \dots \end{bmatrix}$

is a vector of length $\tilde{N} = (m+1)(m+2)/2$ that collects unknown stress parameters of the sub-domain;

- Y^k denotes the kth sub-domain.

It is worth noting that the imposition of equilibrium (with zero body forces, as usually considered in homogenization procedures) inside each sub-domain, the continuity of the stress vector on interfaces and the anti-periodicity of $\mathbf{\sigma n}$ permit directly a strong reduction of the total number of independent stress parameters. The reader is referred to Milani, Lourenço and Tralli (2006a) for further details.

Finally, assemblage operations on the local variables lead to write the stress vector inside each sub-domain as follows:

$$\tilde{\sigma}^{(k)} = \tilde{\mathbf{X}}^{(k)}(\mathbf{y})\tilde{\mathbf{S}}$$

$$k = 1, \dots, \text{number of } sub-domains \tag{4}$$

where $\tilde{\mathbf{S}}$ is a vector of length $\overline{N}$ collecting all the $\overline{N}$ (linearly independent) unknown stress parameters and $\tilde{\mathbf{X}}^{(k)}(\mathbf{y})$ is a $3\mathrm{x}\overline{N}$ coefficients matrix.

In this way, a suitable approximation of the failure surface for unreinforced masonry is obtained solving the linear programming problem (2) with a limited number of optimization unknowns.

Since FRP strips are introduced on masonry already homogenized, equilibrium and admissibility conditions for FRP and for the interface masonry/FRP are discussed in the next Section.

4 Lower and upper bound FE limit analyses on masonry walls reinforced with FRP

4.1 *The lower bound approach*

In this Section, a formulation based on equilibrated and admissible stress fields for the analysis at collapse of FRP reinforced masonry walls is discussed in detail.

According to the lower bound limit theorem for perfectly plastic materials, any statically admissible stress field results in a lower bound estimation of the collapse load. A statically admissible stress field satisfies equilibrium and stress boundary conditions and does not violate the yield criterion.

In this framework, a 2D finite element limit analysis program, based on the equilibrated triangular element by Sloan (1988), has been implemented.

The introduction of FRP reinforcement is treated in what follows making use of the meso-model previously presented.

Let a reinforced masonry wall Ω be considered; it is reinforced by FRP strips characterized by width $l_w^{(k)}$, length $l_s^{(k)}$ and fiber direction identified by the angle $\vartheta_s^{(k)}$, as schematically reported in Figure 4. In what follows, the superscript (k) indicates the kth strip, Ω_m is the unreinforced part of Ω ($\Omega_f \cup \Omega_m = \Omega$), whereas $\mathbf{s}^{(k)}$ and $\mathbf{t}^{(k)}$ represent the vectors parallel and orthogonal to the fiber direction of the kth strip, respectively. A finite element discretization is performed ensuring that there are no elements in which the masonry is only partially reinforced, as shown in Figure 4.

A typical element $E^{(i)} \in \Omega_f$ is regarded as constituted by a central masonry layer of thickness t, subjected to a plane stress state, and by two additional external FRP layers of thickness $s^{(k)}$.
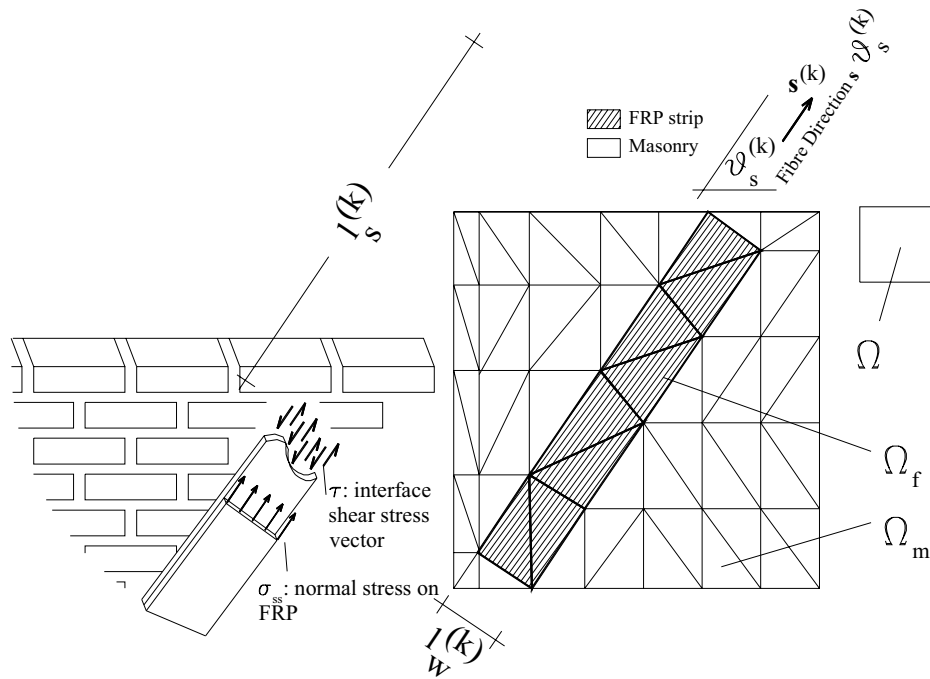
Figure 4 : Geometry of a generic reinforced masonry wall, FE discretization and geometrical properties of FRP strips.
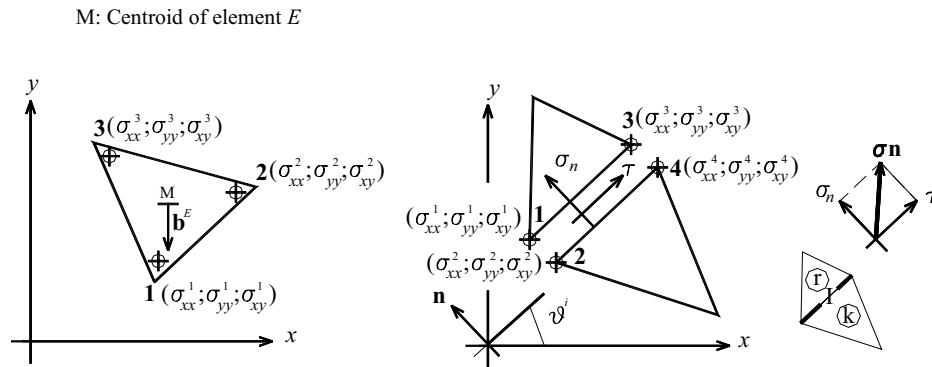
Figure 5 : Linear stress interpolation inside a triangular element and continuity of the stress vector on the edge between adjacent triangles.

It is assumed that only shear stresses $\tau^{(i)}$ with direction $\mathbf{s}^{(k)}$ (see Figure 4) can act at the interface between the masonry and the reinforcement.

For a typical element $E^{(k)} \in \Omega_m$, the stress is assumed varying linearly, in agreement with Sloan (1988) and Poulsen and Damkilde (2000).

In this way, 9 unknown nodal stress parameters are introduced for each element, so that 3 stress parameters (i.e. $\sigma_{xx}^N \quad \sigma_{xy}^N \quad \sigma_{yy}^N$, Figure 5) are associated at each node $N_E^{(k)}$ of the typical element. Statically admissible stress

discontinuities can occur at every edge between adjacent triangles, assuming only the stress vector continuous at interfaces.

For each $E^{(i)} \in \Omega_f$, 2 equilibrium equations for the central masonry layer are imposed taking into account the shear actions due to the presence of the reinforcement strips:

$$t\,div\sigma + t\mathbf{b} - 2\tau = \mathbf{0} \qquad (5)$$

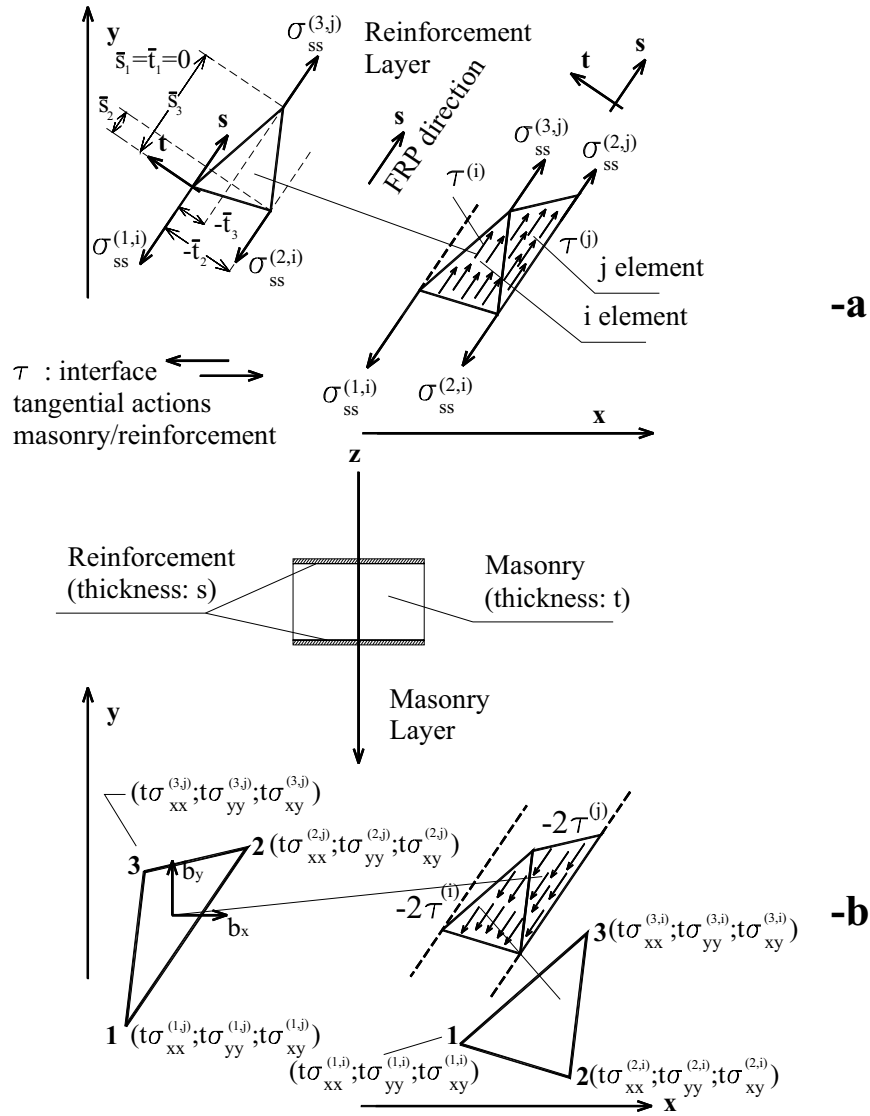where $\mathbf{b}$ denotes the body forces and τ is the interface

Figure 6 : Shear stress distribution on masonry/FRP interface. –a: FRP layer, -b: masonry layer.

shear stress vector. Being the interpolation of the stress linear inside each element, 2 equilibrium equations can be written for each element, one for the x-direction and one for the y-direction. Such equations can be re-written in terms of the nodal unknown stresses and of the shear actions $\tau^{(i)}$ as follows:

$$t\mathbf{A}_{eq}^{(i)}\sigma^{(i)} = -t\mathbf{b}^{(i)} + 2\mathbf{R}\left(\vartheta_S^{(k)}\right)\tau^{(i)} \qquad (6)$$

where:

$$-\mathbf{A}_{eq}^{(i)} = \frac{1}{2A^{(i)}}\begin{bmatrix} \eta_1 & 0 & \zeta_1 & \eta_2 & 0 & \zeta_2 & \eta_3 & 0 & \zeta_3 \\ 0 & \zeta_1 & \eta_1 & 0 & \zeta_2 & \eta_2 & 0 & \zeta_3 & \eta_3 \end{bmatrix},$$

$$\zeta_i = x_j - x_k \quad \eta_i = y_k - y_j \quad i = 1,\ 2,\ 3; \quad k = 2,\ 3,\ 1; \quad j = 3,\ 1,\ 2;$$

- $A^{(i)}$ is the area of the ith element;

$$-\mathbf{R}\left(\vartheta_S^{(k)}\right) = \begin{bmatrix} \cos\left(\vartheta_S^{(k)}\right) & \sin\left(\vartheta_S^{(k)}\right) \end{bmatrix}^T;$$

- $\sigma^{(i)}$, $\mathbf{b}^{(i)}$ represent the 9 nodal unknown stresses and the body forces vector relative to the ith element, respectively.

Regarding the external FRP layers of the typical element $E^{(i)} \in \Omega_f$, only the stress σ_{ss} parallel to the fiber direction is assumed acting, whereas the other stresses are enforced to be zero, i.e. $\sigma_{tt} = \sigma_{ts} = 0$, as reported in Figure 4 and Figure 6. Furthermore, the stress component σ_{ss} is assumed varying linearly inside each FRP element.

Equilibrium is satisfied by imposing the following additional equality constraint inside each element, that corre-

sponds to impose equilibrium along the directions **s**:

$$s \begin{bmatrix} \eta_1^{(i)} & \eta_2^{(i)} & \eta_3^{(i)} \end{bmatrix} \begin{bmatrix} \sigma_{ss}^{(1,i)} & \sigma_{ss}^{(2,i)} & \sigma_{ss}^{(3,i)} \end{bmatrix}^T$$
$$= -2A^{(i)}\tau^{(i)} \qquad (7)$$

where:

- $\eta_q^{(i)} = \bar{t}_k - \bar{t}_j \quad q = 1, 2, 3; \quad k = 2, 3, 1; \quad j = 3, 1, 2$ (Figure 6).

It is worth noting that equilibrium along **t** (orthogonal to **s**) is a-priori satisfied from the hypothesis $\sigma_{tt} = \sigma_{ts} = 0$.

Additional constraints on the nodal stresses of each FRP element are imposed in order to ensure the continuity of the stress vector along the edges of adjacent triangles.

It can be demonstrated (Figure 6-a) that such condition is satisfied by imposing $\sigma_{ss}^{(3,i)} = \sigma_{ss}^{(3,j)}$ and $\sigma_{ss}^{(2,i)} = \sigma_{ss}^{(1,j)}$ where i and j are adjacent elements with common nodes $(3,i) \equiv (3,j)$ and $(2,i) \equiv (1,j)$.

It can be remarked that, in order to fully characterize the behavior of the masonry-FRP reinforced system, the role of delamination and of the limited tensile and compressive strengths of the FRP should be taken into account, i.e. the possible degradation of the interface between masonry and composite and the failure of the composite should be modeled.

Indeed, the delamination of the composite sheet from a masonry element can be regarded as brittle and mainly due to the shear fracture (mode II of fracture) of masonry, rather than to the degradation of the glue (Figure 7). Moreover, a realistic representation of the composite behavior, as reported also by Marfia and Sacco (2001), can be obtained considering a linear elastic response with brittle failure of the FRP, i.e. assuming that the composite collapses under normal actions once that the tensile or the compressive stress reaches a threshold stress f_{df}^+ in tension and f_{df}^- in compression.

Both the delamination and the FRP failure are crucial problems, that obviously can be considered only in an approximate way under the assumption of rigid-plastic behavior of the components, which is the base of limit analysis. In this framework, a treatment of brittle phenomena, such as the brittle failure of the FRP and the masonry-FRP delamination, is precluded.

Admissibility conditions for the reinforcement layers are imposed on σ_{ss} stress for each element in the form $-f_{df}^- \le \sigma_{ss}^{(r,i)} \le f_{df}^+ \ \forall i \ r = 1, 2, 3$ where f_{df}^+ and f_{df}^- are

the failure tensile and compressive strengths of the reinforcement, respectively. In a similar way shear interface actions $\tau^{(i)}$ are supposed to satisfy the inequality $|\tau^{(i)}| \le f_{bd} \ \forall i$ where f_{bd} is the ultimate shear strength of the interface.
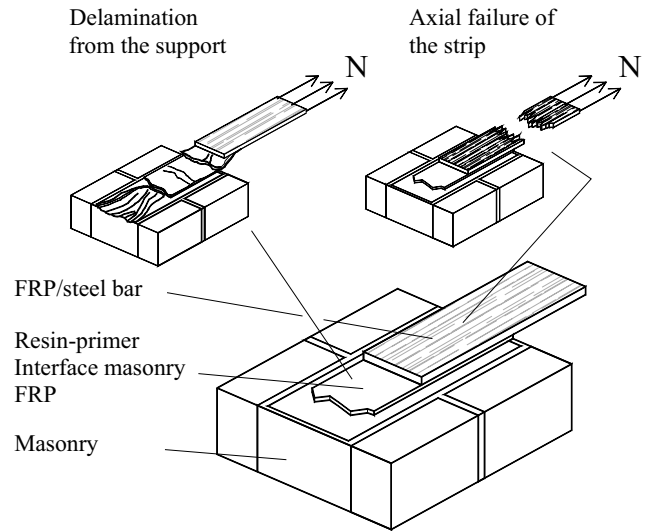

Figure 7 : Possible brittle phenomena for a masonry panel FRP reinforced. Delamination of the strip, failure of the composite.

The Italian CNR DT 200/2004 gives an estimation of f_{bd}, which can be obtained on the basis of the specific fracture energy Γ_{Fd}:

$$\Gamma_{Fd} = \frac{f_{bd}s_f}{\gamma_M} = \frac{c_1}{\gamma_M}\sqrt{f_{mk}f_{mtm}} \quad [f \text{ in N / mm}^2] \qquad (8)$$

where Γ_{Fd} is expressed in $[N / mm]$, c_1 is a parameter usually assumed equal to 0.015 in absence of experimental results, $f_{mtm} = 0.1 f_{mk}$ is the average bricks tensile strength, γ_M is a coefficient that reduces characteristic values to design values and s_f [mm] is the sliding of FRP when a full delamination of the strip occurs. Equation (8) is similar to that proposed in the same code for concrete specimens, for which much more experimentations are actually available.

Equilibrium constraints, boundary conditions on stresses and admissibility conditions for masonry, FRP and interfaces masonry/FRP are suitably assembled and the following linear programming problem is derived at a struc-
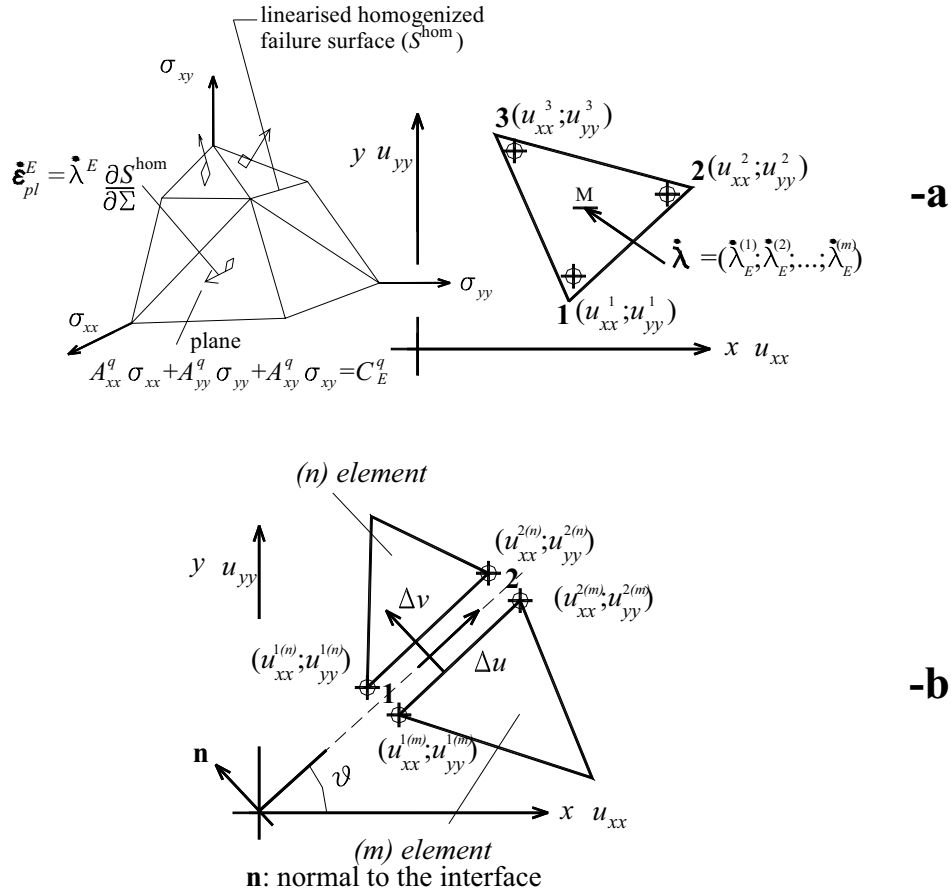
Figure 8 : Field of velocities and plastic dissipation inside an element (-a) and jump of velocities on interfaces.

tural level:

$$
\begin{cases}
\max \{\lambda\} \\[2mm]
\text{subject to } \begin{cases}
\mathbf{A}^{eq} \begin{bmatrix} \mathbf{X}^T & \lambda \end{bmatrix}^T = \mathbf{b}^{eq} \\[2mm]
\mathbf{A}^{in} \begin{bmatrix} \mathbf{X}^T & \lambda \end{bmatrix}^T \le \mathbf{b}^{in}
\end{cases}
\end{cases}
\tag{9}
$$

where λ is the failure load and $\mathbf{X}$ contains the (assembled) masonry in-plane stress parameters, the reinforcement stress vector σ_{ss} and the interfaces shear stress vector τ. Matrices $\mathbf{A}^{eq}$ and $\mathbf{A}^{in}$ collect the coefficients of the equilibrium equations, previously discussed, and the coefficients of admissibility inequalities, respectively, whereas $\mathbf{b}^{eq}$ and $\mathbf{b}^{in}$ are the corresponding right hand sides.

4.2 The upper bound approach

The upper bound approach adopted in this Section is based on the formulation originally developed by Sloan

and Kleeman (1995). Such formulation is based on a triangular discretization of 2D domains and on the introduction of discontinuities of the velocity field along the edges of adjacent triangles. It has been shown (Milani Lourenço Tralli 2006b) that the definition of kinematically admissible velocity fields with discontinuities at interfaces is adequate for purely cohesive or cohesive-frictional materials, which is the case of masonry.

For each element E, two velocity unknowns per node i, say u_{xx}^i and u_{yy}^i (one along x and one along y, see Figure 8-a) are introduced, so that the velocity field is linear inside each element, whereas the strain rate field is constant.

Jumps of velocities at interfaces are supposed to vary linearly. Hence, four unknowns collected in the vector $\Delta \mathbf{u}^I = [\Delta v_1 \ \Delta u_1 \ \Delta v_2 \ \Delta u_2]^T$ are introduced at each interface; the components of the vector $\Delta \mathbf{u}$ represent the normal Δv_i and tangential Δu_i jumps of velocities (with respect to the discontinuity direction) evaluated at nodes $i = 1$ and $i = 2$ of the interface (see Figure 8-b).
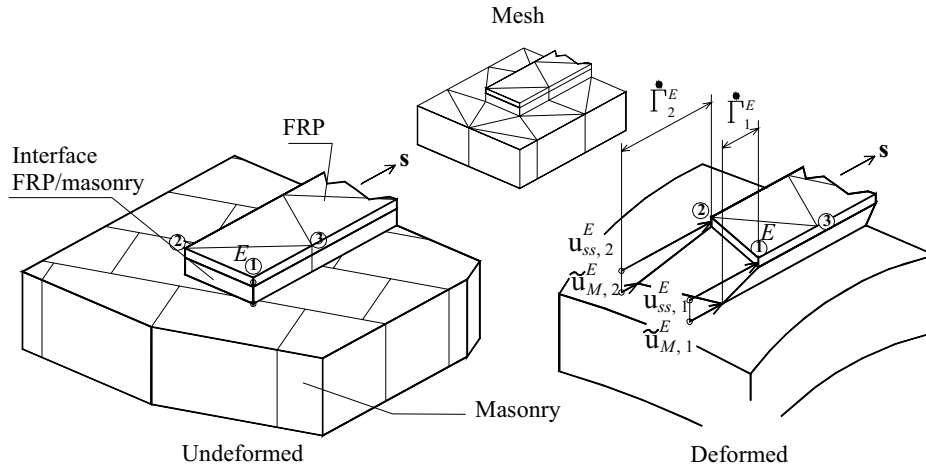
Figure 9 : Field of velocities on FRP and on the interfaces masonry/FRP.

For any pair of nodes lying on the interface between the two adjacent triangles m and n, the tangential and normal velocity jumps can be written in terms of the Cartesian nodal velocities of elements $m-n$; thus, four linear equations for each interface are obtained assuming the form:

$$\mathbf{A}_{11}^{eq}\mathbf{u}^{Em} + \mathbf{A}_{12}^{eq}\mathbf{u}^{En} + \mathbf{A}_{13}^{eq}\Delta\mathbf{u}^I = \mathbf{0} \tag{10}$$

where $\mathbf{u}^{Em}$ and $\mathbf{u}^{En}$ are vectors with six components, collecting the velocities of elements m and n, respectively, and $\mathbf{A}_{11}^{eq}$, $\mathbf{A}_{12}^{eq}$, $\mathbf{A}_{13}^{eq}$ are matrices which depend only on ϑ angle (Figure 8-b). Further kinematic variables are introduced in order to model, in the framework of the upper bound approach, the effect of the FRP strengthening (Figure 7). The sliding mode between masonry and FRP is modeled considering a linear field $\dot{\Gamma}^E$ of interfacial velocities inside each element $E^{(i)} \in \Omega_f$, i.e. 3 further velocity unknowns per element are introduced. On the other hand, a possible plastic dissipation due to the failure of the FRP subjected to axial stresses is taken into account introducing a linear field $\mathbf{u}_{ss}$ of velocities inside each FRP element, acting along the fiber direction defined by the angle $\vartheta_s^{(k)}$.

As it is shown in Figure 9, the following compatibility constraint involving $\mathbf{u}_{ss}$, $\dot{\Gamma}^E$ and $\tilde{u}_{M,i}^E$ occur for each node $i \in E^{(i)}$, with $E^{(i)} \subset \Omega_f$:

$$u_{ss,i}^E = \tilde{u}_{M,i}^E + \dot{\Gamma}_i^E \tag{11}$$

Where $\tilde{u}_{M,i}^E$ represents the velocity in the brickwork, evaluated along strips directions at node i.

After classical assemblage operations, a linear programming problem is obtained, which results to be analogous to that reported by Milani, Lourenço and Tralli (2006b) and in which the objective function consists in the minimization of the total internal power dissipated:

$$\begin{cases} \min \left\{ \mathbf{C}_E^T\dot{\lambda}^{E,ass} + \mathbf{C}_I^T\dot{\lambda}^{I,ass} \right. \\ \qquad \left. + \mathbf{C}_{I^{FRP}}^T\dot{\lambda}^{I^{FRP},ass} + \mathbf{C}_{FRP}^T\dot{\lambda}^{FRP,ass} \right\} \\ \\ \text{such that} \begin{cases} \tilde{\mathbf{A}}^{eq}\mathbf{U} = \tilde{\mathbf{b}}^{eq} \\ \\ \dot{\lambda}^{I,ass} \geq \mathbf{0} \quad \dot{\lambda}^{E,ass} \geq \mathbf{0} \\ \\ \dot{\lambda}^{I^{FRP},ass} \geq \mathbf{0} \quad \dot{\lambda}^{FRP,ass} \geq \mathbf{0} \end{cases} \end{cases} \tag{12}$$

where:

- $\mathbf{C}_E^T$ and $\mathbf{C}_I^T$ are the assembled right-hand sides of the inequalities which determine the linearized failure surface of the homogenized material in continuum and in the interfaces, respectively;

- $\mathbf{C}_{I^{FRP}}^T$ and $\mathbf{C}_{FRP}^T$ are the assembled right-hand sides of the inequalities which determine the linearized failure surfaces of the interface masonry/FRP and of FRP, respectively;

- $\mathbf{U} = \begin{bmatrix} \mathbf{u}_M & \dot{\lambda}^{E,ass} & \Delta\mathbf{u}^{I,ass} & \dot{\lambda}^{I,ass} \\ & \dot{\Gamma} & \dot{\lambda}^{I^{FRP},ass} & \mathbf{u}_{ss} & \dot{\lambda}^{FRP,ass} \end{bmatrix}$

is the assembled vector of kinematic unknowns and collects the vectors of assembled nodal velocities $\mathbf{u}_M$, elements plastic multiplier rates $\dot{\lambda}^{E,ass}$, jump of velocities on

Mortar   Bricks

-a   **-b**
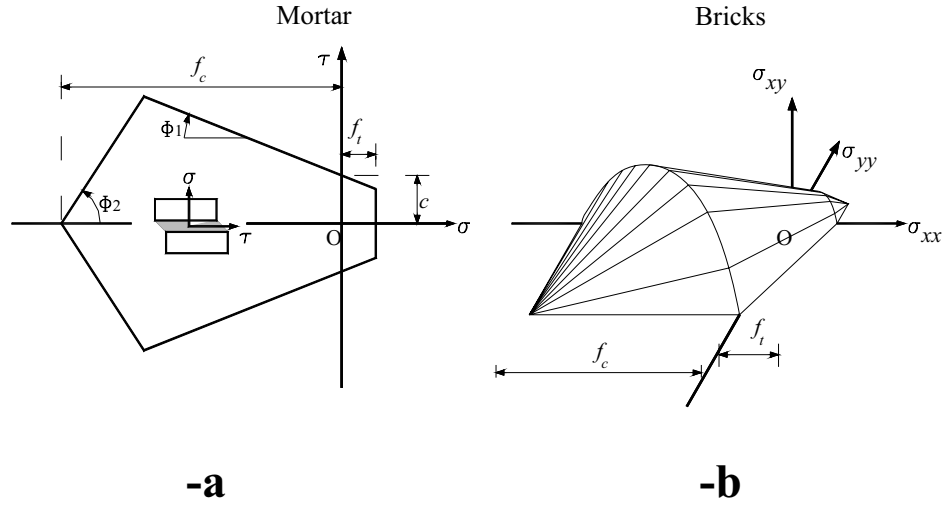
Figure 10 : Strength domains for the constituent materials; interface strength domain for mortar joints (-a) and Mohr-Coulomb in plane stress for bricks (-b).

interfaces $\Delta \mathbf{u}^{I,ass}$, interface plastic multiplier rates $\dot{\lambda}^{I,ass}$, masonry/FRP interface velocities $\dot{\boldsymbol{\Gamma}}$, masonry/FRP interface plastic multiplier rates $\dot{\lambda}^{I^{FRP},ass}$, FRP velocities $\mathbf{u}_{ss}$ and FRP plastic multiplier rates $\dot{\lambda}^{FRP,ass}$.

It is worth noting that $\mathbf{C}_{I^{FRP}}^T \dot{\lambda}^{I^{FRP},ass}$ and $\mathbf{C}_{FRP}^T \dot{\lambda}^{FRP,ass}$ in equation (12) represent the total power dissipated on masonry/FRP interfaces and on FRP, respectively. Within each triangle E of area A, it can be shown that the power dissipated on the interface masonry/FRP is expressed by the linear equation:

$$P_{I^{FRP}}^E = \frac{A}{3} \sum_{q=1}^{3} f_{bd} \left(\dot{\lambda}_{E_{I^{FRP}}}^{+(q)} + \dot{\lambda}_{E_{I^{FRP}}}^{-(q)} \right) \tag{13}$$

where $\dot{\lambda}_{E_{I^{FRP}}}^{+(q)}$ and $\dot{\lambda}_{E_{I^{FRP}}}^{-(q)}$ are the plastic multiplier rates of the triangle E associated to node q and corresponding to plastic dissipation on interfaces when $\tau^{(q)} = f_{bd}$ and $\tau^{(q)} = -f_{bd}$ respectively.

In a similar way, the power dissipated on the FRP can be written as:

$$P_{FRP}^E = \frac{A}{3} \sum_{q=1}^{3} \left(f_{df}^+ \dot{\lambda}_{E_{FRP}}^{+(q)} + f_{df}^- \dot{\lambda}_{E_{FRP}}^{-(q)} \right) \tag{14}$$

where $\dot{\lambda}_{E_{FRP}}^{(q)}$ and $\dot{\lambda}_{E_{FRP}}^{-(q)}$ are the plastic multiplier rates of the triangle E associated to node q and corresponding to plastic dissipation of FRP when $\sigma_{ss}^{(q)} = f_{df}^+$ and $\sigma_{ss}^{(q)} = f_{df}^-$ respectively.

Finally, $\tilde{\mathbf{A}}^{eq}$ and $\tilde{\mathbf{b}}^{eq}$ in equation (12) denote the overall constraints matrix and constraints right hand sides, respectively, and they collect velocity boundary conditions, relations between velocity jumps on interfaces and elements velocities, constraints for plastic flow in velocity discontinuities, constraints for plastic flow in continuum and compatibility conditions between $\mathbf{u}_{ss}$, $\dot{\boldsymbol{\Gamma}}$ and $\mathbf{u}_M$.

5 Comparison between experimental evidences and numerical results for masonry walls reinforced with FRP

In this Section, the accuracy of the results obtained by means of the numerical model proposed in Section 3 is assessed through a comparison with experimental results.

For each tested panel, force-displacement curves, crack patterns and FRP strips delamination were registered during the experimental campaign.

The first and second analyzed structural examples consist in masonry panels acting as deep beams (Pan B and Pan C series, Figure 11), equipped with a horizontal and a symmetrically disposed diagonal reinforcement, respectively. The third case is represented by a masonry wall with a central square opening subjected to a vertical concentrated load applied on the top edge (PanWin B series, Figure 18), strengthened with two diagonal strips disposed immediately under the load.

Failure loads (both upper and lower bounds), stress distribution at collapse on critical sections and failure mech-
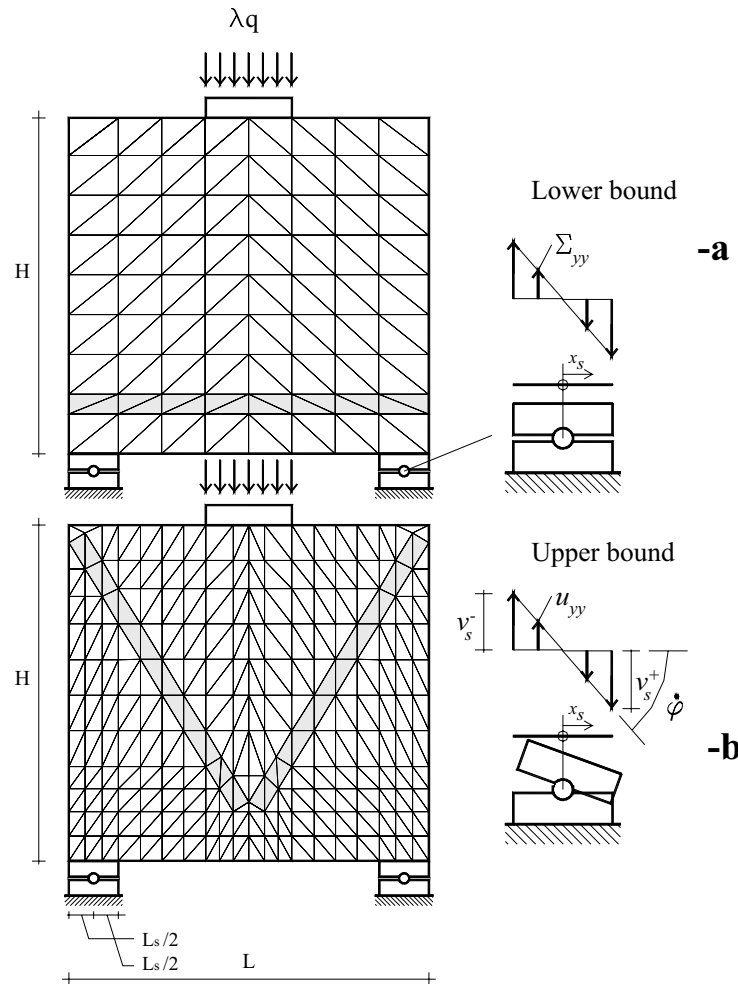
Figure 11 : Mesh used for Pan B series (-a) and Pan A and Pan C series (-b).

anisms are provided by the previously discussed numerical procedure. For all the analyzed cases, a further comparison with experimental results for the same unreinforced panels is reported (Pan A series and PanWin A series, respectively) in order to predict the failure loads increase due to the strengthening introduction.

5.0.1 Mechanical properties adopted

In the framework of limit analysis, a linearized frictional-type failure surface is chosen for joints reduced to interfaces, as shown in Figure 10-a, according to Lourenço and Rots (1997) and Sutcliffe, Yu and Page (2001).

Mechanical characteristics of mortar at failure are shown in Table 6. It is worth noting that joints compressive strength f_c adopted in the numerical simulations is assumed equal to the experimental masonry compressive strength value, since 3D effects and brittle behavior of

**Table 6** : Mechanical characteristics adopted for mortar joints reduced to interfaces.

f_c	$f_t (c = 1.6 f_t)$	Φ_1	Φ_2
6.76	0.2	36 °	30 °
MPa	MPa	-	-

bricks can not be reproduced with the proposed rigid plastic homogenization approach, as discussed by Milani, Lourenço and Tralli (2006a).

Finally, in accordance with experimental data, a Mohr-Coulomb plane stress failure criterion is adopted for brick, with $f_c = 15.66\,N/mm^2$ and $f_t = 1/10 f_c$ (Figure 10-b).

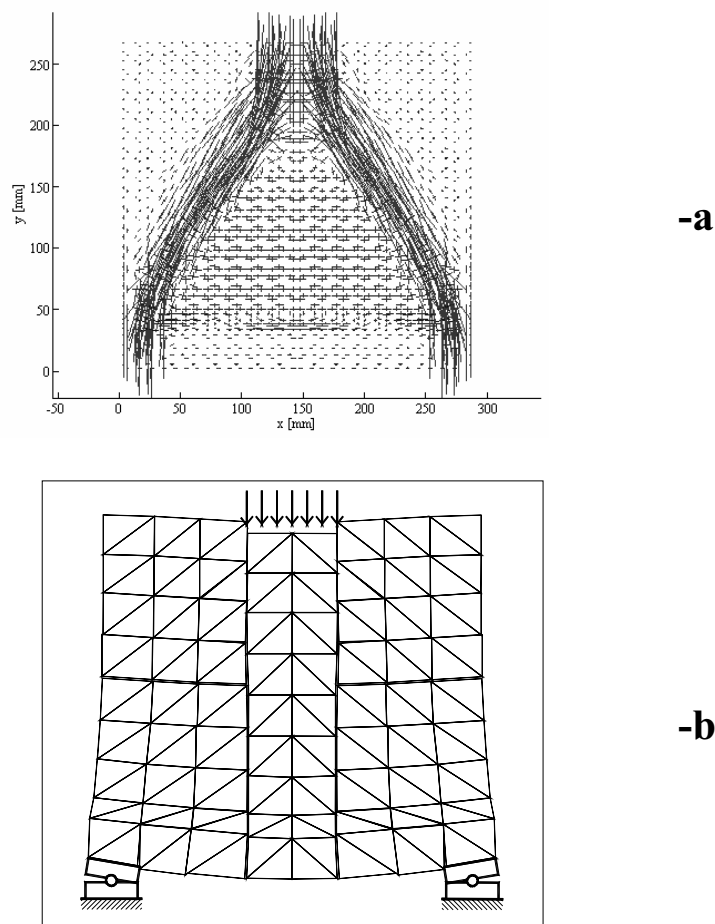**Force-Displacement curves point A (Pan A series)**
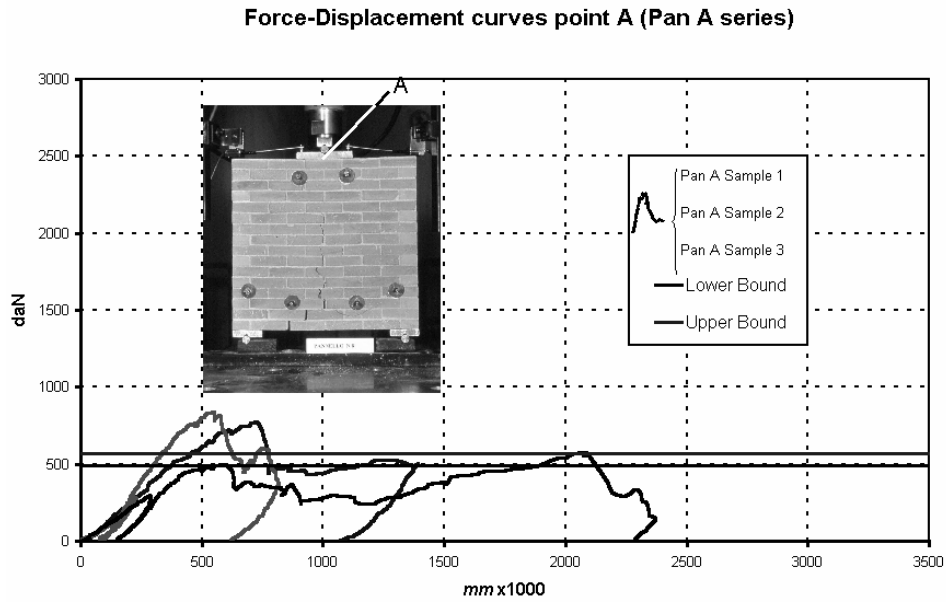
Figure 12 : Pan A series, comparison between failure loads obtained by means of the upper and lower bound approach and experimental force-displacements curves.
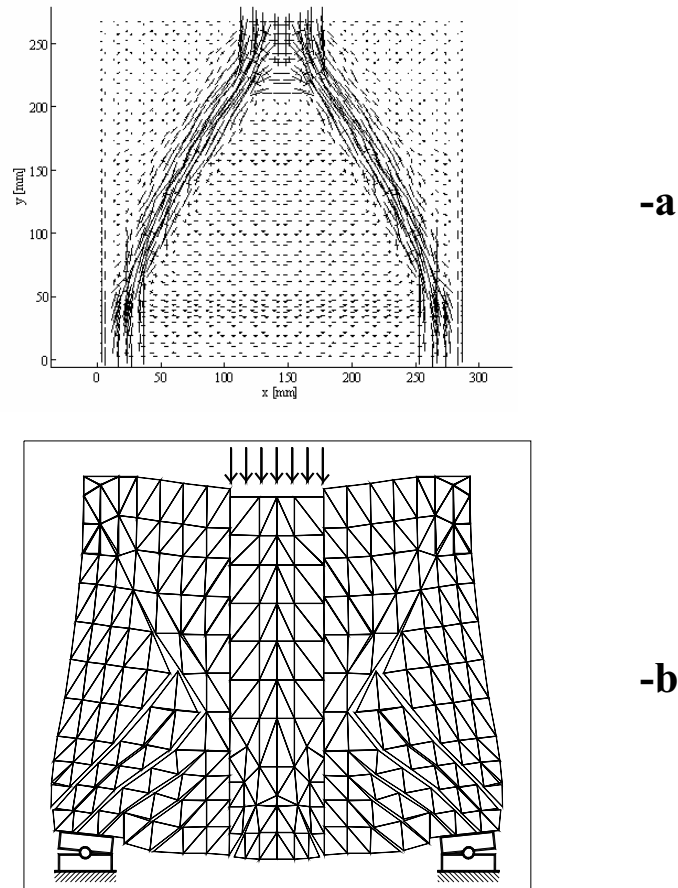
Figure 13 : Stress distribution at collapse (-a) and field of velocities at collapse (-b), series Pan A.
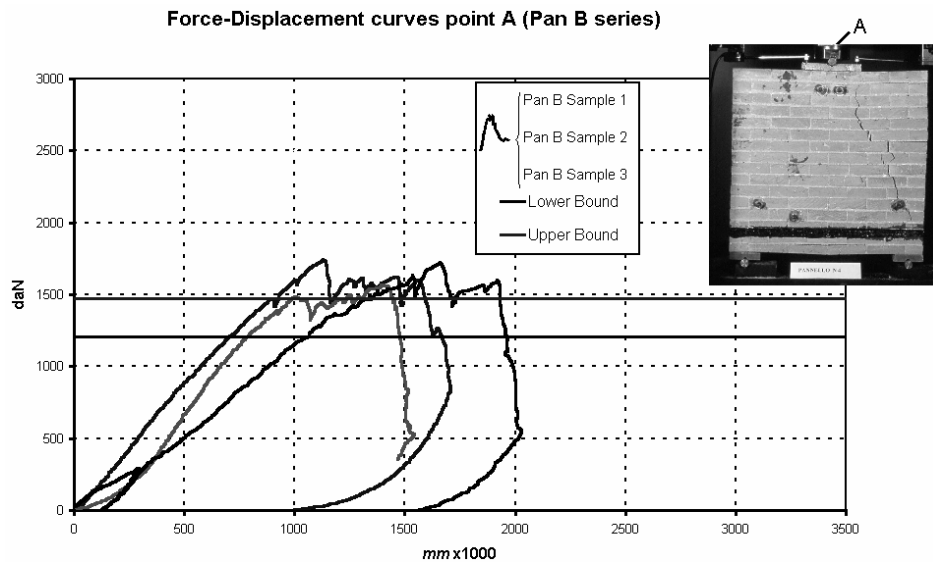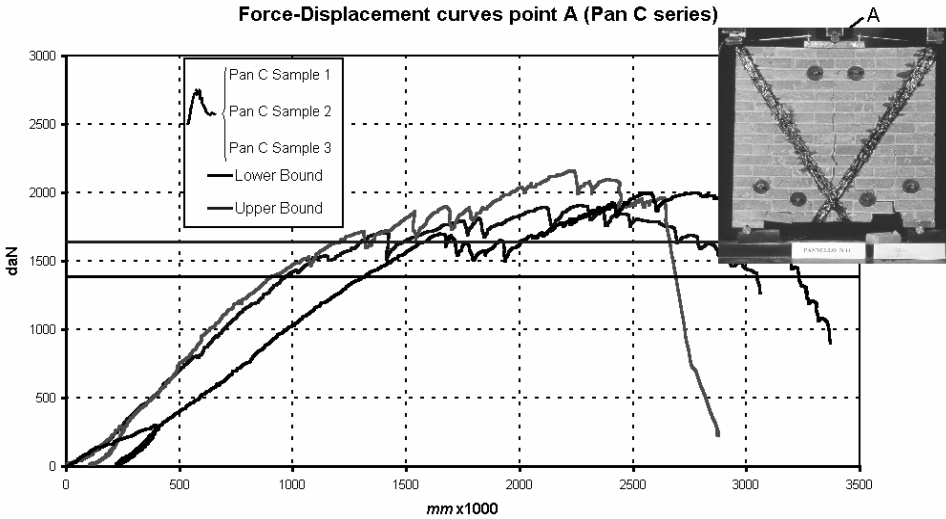
Figure 14 : Pan B series, comparison between failure loads obtained by means of the upper and lower bound approach and experimental force-displacements curves.

Figure 15 : Stress distribution at collapse (-a) and field of velocities at collapse (-b), series Pan B.

Figure 16 : Pan C series, comparison between failure loads obtained by means of the upper and lower bound approach and experimental force-displacements curves.
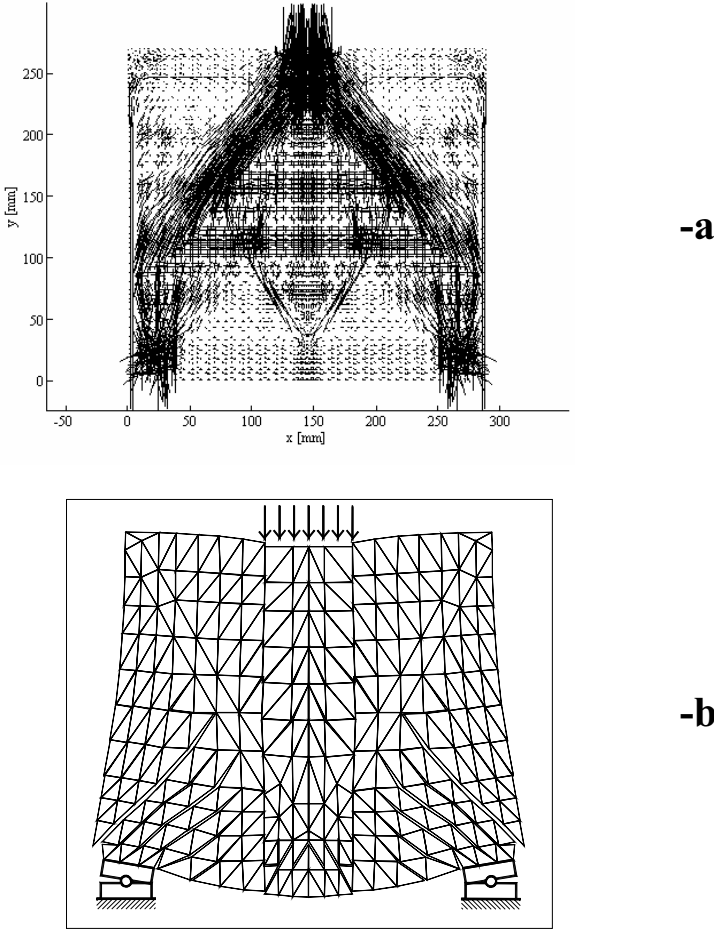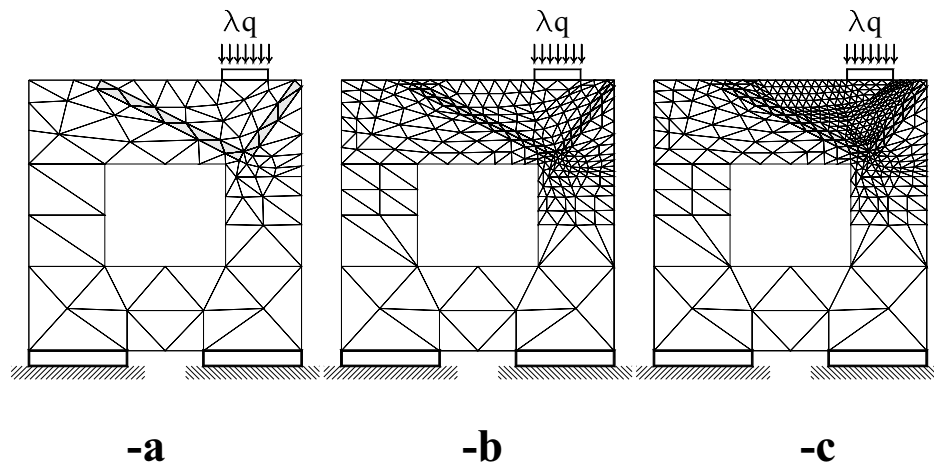

Figure 17 : Stress distribution at collapse (-a) and field of velocities at collapse (-b), series Pan C.

Figure 18 : Meshes used for the the analysis of PanWin A and PanWin B. –a: Mesh 1 (121 elements); -b: Mesh 2 (422 elements); -c: Mesh 3 (706 elements).

5.1 Panels Pan A Pan B and Pan C

The FE discretizations adopted for the analyses of Pan B and Pan C series are reported in Figure 11-a and -b, respectively.

For Pan A, without reinforcement, the same mesh used for Pan C has been adopted. As shown in Figure 11 the symmetrical steel supports disposed at the base of the wall preclude only vertical/horizontal displacements, whereas rotation is allowed by the introduction of little steel rollers immediately under the supports.

In the FE limit analysis models, this is taken into account by imposing for the lower bound the moment on the supports $t \int_{-L_s/2}^{L_s/2} \Sigma_{yy} x_s dx_s = 0$, where L_s is the support length, t is masonry thickness, Σ_{yy} is the vertical stress in correspondence of the edges of the elements adjacent to the support and x_s is a horizontal abscissa measuring support length with origin in correspondence of the middle of the support (Figure 11-a).

In a dual manner with respect to the lower bound approach, in the upper bound approach, a rotation velocity $\dot{\varphi}$ is allowed on the supports constraining vertical velocities of the nodes belonging to the support to have a linear dependence on vertical velocities v_s^- and $v_s^+ = -v_s^-$ of the nodes with abscissa $x_s = \pm L_s/2$, so that $\dot{\varphi} = 2v_s^-/L_s$ (Figure 11-b).

It is worth noting that experimental evidences show a crack pattern with a preferentially oriented vertical fracture line, due to the reduced masonry tensile strength.

Furthermore a relatively ductile behavior of the specimens is observed.

In Figure 12 a comparison between failure loads obtained by means of the upper and lower bound approaches and experimental force-displacements curves is reported for Pan A series.

Principal stress distribution at collapse and failure mechanism are reported in Figure 13-a and -b. It is evident the internal definition of a simple two-strut model in the masonry panel, that allows to transfer the load from the point of application to the supports.
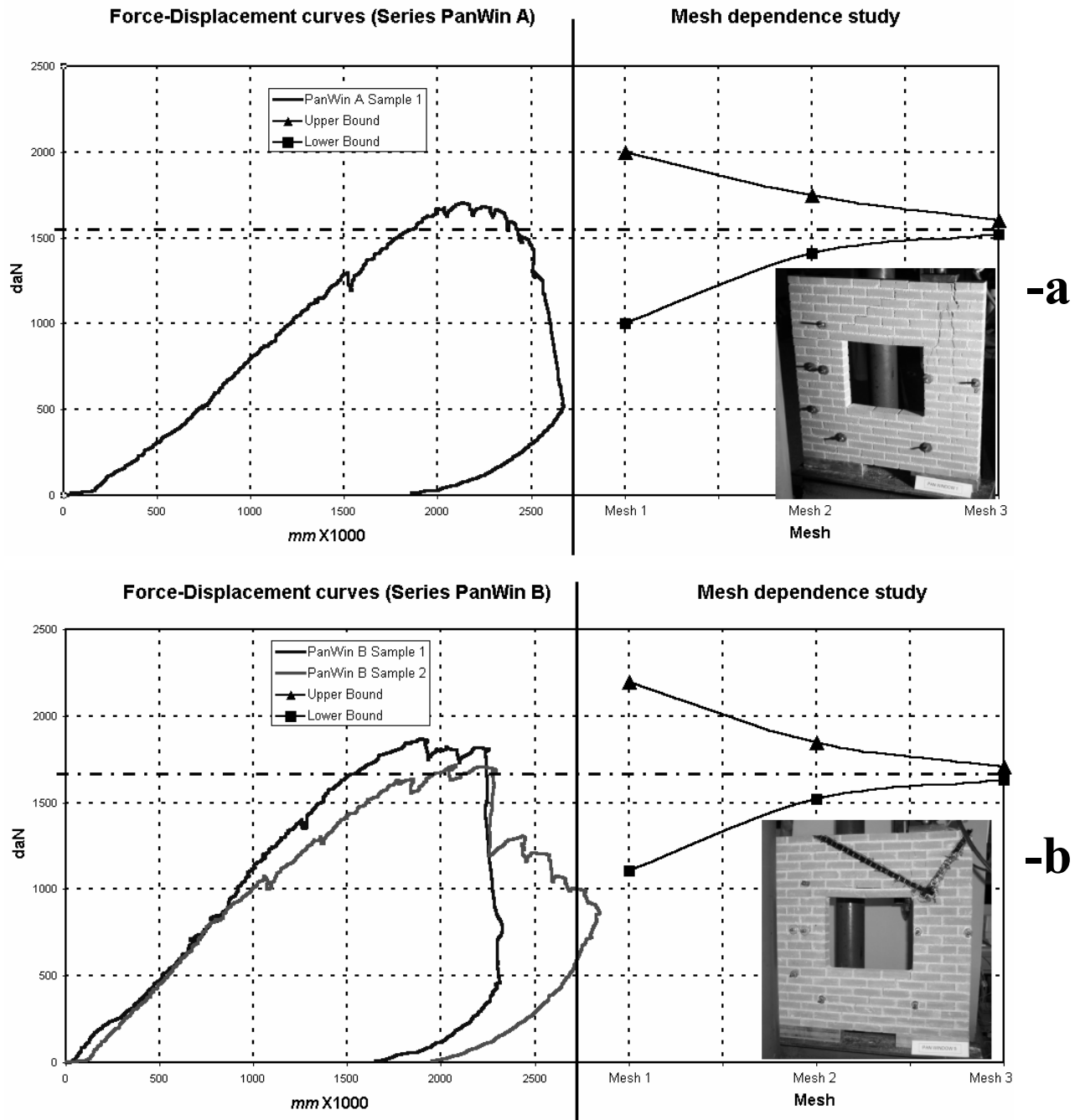
In Figure 14 a comparison between a numerical evaluation of the failure loads and experimental force-displacements curves is reported for Pan B series.

The experimental crack pattern presents almost symmetrical diagonal fracture lines (perpendicular to the compressed struts) and a decohesion of the FRP strip in correspondence of its terminal parts is observed. Furthermore, the experimental data show a quite limited ductile behavior of the specimens.

As the FE lower and upper bound simulations show (Figure 15-a and -b), the horizontal strip acts as a tie. Even though the two-strut model of the unreinforced case remains essentially unchanged, both the compressed sections increase as well the intensity.

Finally, in Figure 16 and Figure 17 the same comparisons shown for Pan B are reported for Pan C series.

In this case the experimental crack pattern presents vertical and diagonal fracture lines combined with a delam-

Figure 19 : Comparison between force displacement experimental curves and failure loads numerically evaluated. –a: unreinforced case (PanWin A series); –b: reinforced case (PanWin B series).

ination of the FRP strips at the lower extremes. On the other hand, the principal stress distribution at collapse and the failure field of velocities provided by the numerical simulations result in a change both of the direction of the compressed struts and in the failure mechanism. The deformed shape at collapse shows compression near the

supports, shear under the load and delamination of the diagonal reinforcement.

The comparisons between numerical failure loads and experimental force-displacement curves (Figure 12, Figure 14 and Figure 16) show that the presented model is able to predict the strong increase of the ultimate load,

-a   **-b**
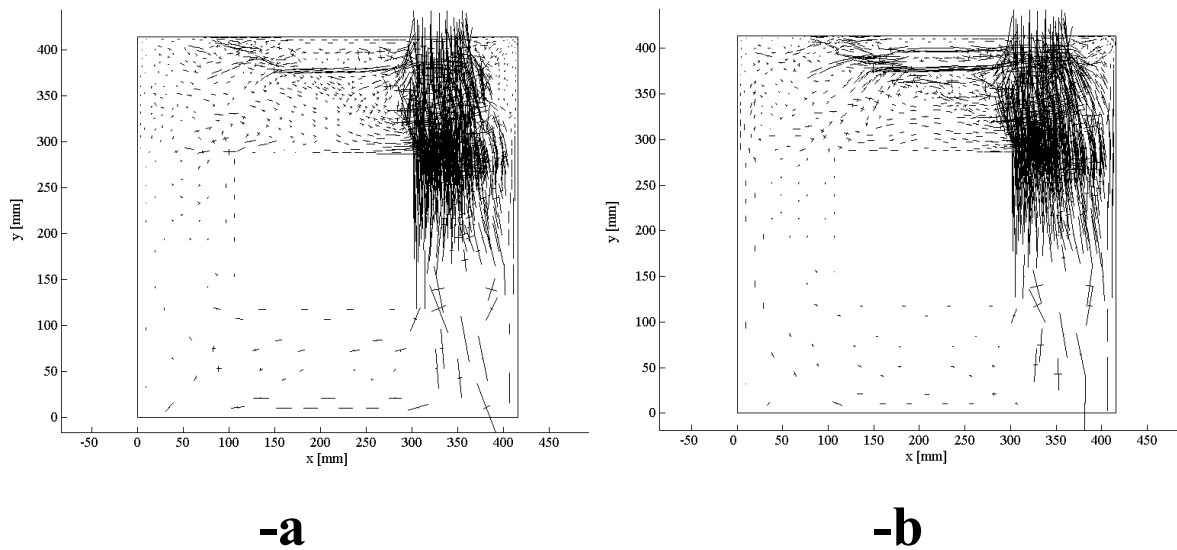
Figure 20 : Principal stress distribution at collapse. –a: unreinforced case (PanWin A series); –b: reinforced case (PanWin B series).

-a   **-b**
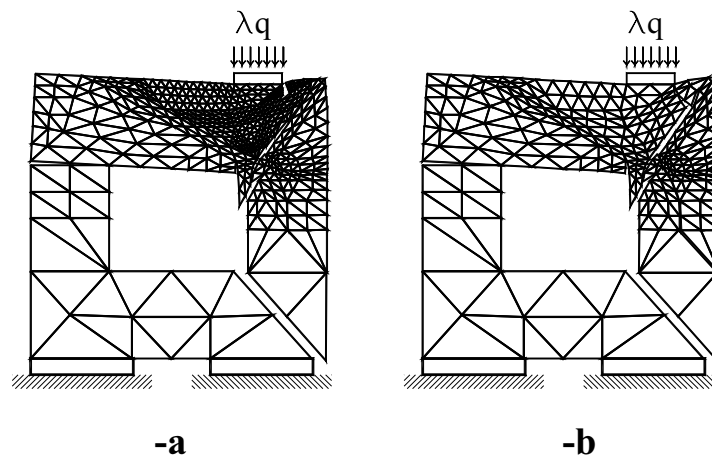
Figure 21 : Field of velocities at collapse. –a: unreinforced case (PanWin A series); –b: reinforced case (PanWin B series).

which results to be 150% greater than the one obtained for the unreinforced case, both for the diagonal and horizontal reinforcements. On the other hand, experimentation shows that Pan B series presents a vertical displacement at collapse approximately one half with respect to Pan C series, which exhibits a relatively ductile behavior.

5.2   *PanWin A and PanWin B series*

Three meshes have been adopted both for PanWin A and PanWin B series, as shown in Figure 18, in order to study mesh dependence of the model when lower and upper bound FE limit analyses are performed.

Experimental tests demonstrate that the introduction of FRP does not determine, in this case, a significant change of the failure load. This is kept by the proposed numerical model. Furthermore, the experimental crack pattern observed in the unreinforced panel presents almost vertical fracture lines and experimental evidences show that the introduction of FRP reinforcement does not vary the direction of cracks significantly. Besides, in PanWin B series a delamination of the FRP strips in correspondence of the lower extremes is observed.

In Figure 19–a and –b, a comparison between force-displacement experimental curves and failure upper and

lower bound loads obtained for progressively refined meshes, is reported for the unreinforced and reinforced panels, respectively.

Principal stress distributions at collapse provided by the FE lower bound approach are shown in Figure 20–a and –b for the unreinforced and reinforced case, respectively.

Finally, in Figure 21-a and -b, failure mechanisms obtained with the upper bound approach are reported for the unreinforced and reinforced case, respectively.

As it is possible to note, numerical simulations confirm that both stress distribution at collapse and failure field of velocities remain essentially unchanged after the introduction of the reinforcement. In particular, Figure 21 shows that the collapse mechanism of the panel does not vary significantly, so justifying the limited increase of the failure load.

References

Cecchi, A.; Milani, G.; Tralli, A. (2004): In-plane loaded CFRP reinforced masonry walls: mechanical characteristics by homogenisation procedures. *Composites Science and Technology*, vol. 64, pp. 2097-2112.

CNR DT 200/2004 (2004): Istruzioni per la progettazione, l'esecuzione e il controllo di interventi di consolidamento statico mediante l'utilizzo di compositi fibrorinforzati (Instructions for the design, execution and control of strengthening interventions by means of fiber reinforced composites).

Corradi, M.; Borri, A.; Vignoli, A. (2002): Strengthening techniques tested on masonry structures struck by the Umbria-Marche earthquake of 1997-1998. *Construction and Building Materials*, vol. 16, pp. 229-239.

de Buhan, P.; de Felice, G. (1997): A homogenisation approach to the ultimate strength of brick masonry. *J. Mech, Phys. Solids*, vol. 45 (7), pp. 1085-1104.

Di Tommaso, A. (ed) (2000): Mechanics of masonry structures strengthened with FRP materials, Libreria Cortina, Padova, Italy.

D.M. 3/6/1968 (1968): Nuove norme sui requisiti di accettazione e modalità di prova dei cementi (New norms on the acceptance requisites and tests set up for cements).

D.M. 20/11/1987 (1987): Norme tecniche per la progettazione, esecuzione e collaudo degli edifici in muratura e per il loro consolidamento (Technical norms for the design, execution and test of masonry buildings and for their consolidation).

Limam, O.; Foret, G.; Ehrlacher, A. (2003): RC two way slabs strengthened with CFRP strips: experimental study and a limit analysis approach. *Composites Structures*, vol. 60, pp. 467-471.

Lourenço, P. B.; Rots, J. (1997): A multi-surface interface model for the analysis of masonry structures. *Jour. of Eng. Mech. ASCE*, vol. 123 (7), pp. 660-668.

Luciano, R.; Sacco, E. (1998): Damage of masonry panels reinforced by FRP sheets. *Int. Journ. Sol. Struct.*, vol. 35, pp. 1723-1741.

Marfia, S.; Sacco E. (2001): Modeling of reinforced masonry elements. *Int. Journ. Sol. Struct.*, vol. 38, pp. 4177-4198.

Milani, G.; Lourenço P. B.; Tralli, A. (2006a): Homogenised limit analysis of masonry walls. Part I: failure surfaces. *Comp. Struct.*, vol. 84, pp. 166C180.

Milani, G.; Lourenço P. B.; Tralli, A. (2006b): Homogenised limit analysis of masonry walls. Part II: structural examples. *Comp. Struct.*, vol. 84, pp. 181C195.

Nanni, A.; Tumialan, J. G. (2003): Fiber-reinforced composites for the strengthening of masonry structures. *Structural Engineering International*, vol. 13 (4).

Olsen P.C. (2000): Rigid-plastic finite element analysis of steel plates, structural girders and connections. *Comp. Meth. Appl. Mech. Eng.*, vol. 191, pp. 761-781.

Poulsen, P. N.; Damkilde, L. (2000): Limit state analysis of reinforced concrete plates subjected to in-plane forces. *Int. Jour. Sol. Struct.*, vol. 37, pp. 6011-6029.

Schwegler, G. (1994): Masonry construction strengthened with composites in seismically endangered zone. *10th European Conference on Earthquake Engineering*, Wien, pp. 2299-2303.

Sloan, S. W. (1988): Lower bound limit analysis using finite elements and linear programming. *Int. Jour. Num. An. Meth. Geomech.*, vol. 12, pp. 61-77.

Sloan, S. W.; Kleeman, P. W. (1995): Upper bound limit analysis using discontinuous velocity fields. *Comp.*

Meth. Appl. Mech. Eng., vol. 127 (1-4), pp. 293-314.

Suquet, P. (1983): Analyse limite et homogeneisation. *C.R. Acad Sci*, Paris 296 (Serie II), pp. 1355 –8.

Sutcliffe, D. J.; Yu, H. S.; Page, A. W. (2001): Lower bound limit analysis of unreinforced masonry shear walls. *Comp. Struct.*, vol. 79, pp. 1295-1312.

Triantafillou, T. C.; Fardis, M. N. (1997): Strengthening of historic masonry structures with composite materials. *Int. Jour. of Materials and Structures*, vol. 30.